Development 138, 4511-4522 (2011) doi:10.1242/dev.063867

Rhou maintains the epithelial architecture and facilitates differentiation of the foregut endoderm

David A. F. Loebel[1,2], Joshua B. Studdert[1], Melinda Power[1], Tania Radziewic[1], Vanessa Jones[1], Leigh Coultas[3], Yvette Jackson[1,4], Renuka S. Rao[1,*], Kirsten Steiner[1], Nicolas Fossat[1,2], Lorraine Robb[3] and Patrick P. L. Tam[1,2,†]

SUMMARY

Rhou encodes a Cdc42-related atypical Rho GTPase that influences actin organization in cultured cells. In mouse embryos at early-somite to early-organogenesis stages, *Rhou* is expressed in the columnar endoderm epithelium lining the lateral and ventral wall of the anterior intestinal portal. During foregut development, *Rhou* is downregulated in regions where the epithelium acquires a multilayered morphology heralding the budding of organ primordia. In embryos generated from *Rhou* knockdown embryonic stem (ES) cells, the embryonic foregut displays an abnormally flattened shape. The epithelial architecture of the endoderm is disrupted, the cells are depleted of microvilli and the phalloidin-stained F-actin content of their sub-apical cortical domain is reduced. *Rhou*-deficient cells in ES cell-derived embryos and embryoid bodies are less efficient in endoderm differentiation. Impaired endoderm differentiation of *Rhou*-deficient ES cells is accompanied by reduced expression of c-Jun/AP-1 target genes, consistent with a role for Rhou in regulating JNK activity. Downregulation of *Rhou* in individual endoderm cells results in a reduced ability of these cells to occupy the apical territory of the epithelium. Our findings highlight epithelial morphogenesis as a required intermediate step in the differentiation of endoderm progenitors. In vivo, *Rhou* activity maintains the epithelial architecture of the endoderm progenitors, and its downregulation accompanies the transition of the columnar epithelium in the embryonic foregut to a multilayered cell sheet during organ formation.

KEY WORDS: Rho GTPase, Rhou, Endoderm, Epithelial morphogenesis, Organ bud formation, Mouse

INTRODUCTION

The definitive endoderm (DE) is a transient embryonic epithelial cell layer that forms the linings of the digestive and respiratory systems as well as organs for gas exchange, digestion and absorption, and removal of metabolic end products. The progenitors of the anterior DE, which underlie the head folds, are derived from epiblast cells anterior to the distal tip of the mid- to late-streak stage embryo (Lawson et al., 1986; Tam et al., 2007). Cells of the anterior DE form the foregut (Franklin et al., 2008; Tremblay and Zaret, 2005), which contributes to the lung, stomach, oesophageal and tracheal epithelia, as well as the liver, pancreas, thyroid and thymus (Zorn and Wells, 2009).

In a transcriptome analysis of the foregut endoderm of early-somite stage mouse embryos, we identified *Rhou* (also known as *Wrch1*), which codes for a Rho GTPase with 70% sequence similarity to Cdc42, among the genes that are preferentially expressed in the endoderm of the anterior intestinal portal. Rhou activity has been shown to influence the actin cytoskeleton, cell shape and behaviour in cultured cells. In fibroblasts, Rhou overexpression reduces the number of lamellipodia and the actin content of stress fibres (Saras et al., 2004) but enhances filopodia formation (Saras et al., 2004; Tao et al., 2001) and cell motility (Ory et al., 2007). In HeLa cells, Rhou localizes to focal adhesions and its overexpression promotes the disassembly of focal adhesions and increases cell motility (Chuang et al., 2007). Consistent with the cell culture results, in *Xenopus* embryos, in which *Rhou* is expressed in migrating cranial neural crest cells, *Rhou* knockdown impairs cell migration (Fort et al., 2011). In MDCK (canine kidney epithelial) cells, overexpression of *Rhou* disrupts tight junction formation and the distribution of F-actin, and depletion of *Rhou* disrupts lumen formation in cysts (Brady et al., 2009). The findings of these studies suggest that Rhou plays a role in regulating epithelial cell shape and structure and modulating cellular behaviour.

We have investigated the expression and function of *Rhou* in the development of the foregut endoderm in the mouse. We generated embryonic stem (ES) cell lines in which *Rhou* activity was stably knocked down. Analysis of differentiation of the *Rhou*-knockdown cells in vitro revealed a defect in endodermal lineage differentiation. In ES cell-derived embryos, knockdown of *Rhou* altered the epithelial architecture and impaired the differentiation of the foregut endoderm. Focal electroporation of *Rhou* small hairpin RNA (shRNA) constructs into the endoderm pinpointed a cell autonomous role for Rhou in maintaining epithelial structure. Our findings highlight a requirement for *Rhou* activity in maintaining the F-actin-related cytoskeletal organization of the foregut endoderm, which is required for maintaining proper tissue structure and facilitating cell differentiation, and present a mechanistic paradigm that the transition of epithelial architecture constitutes a critical step in the process of controlling the formation of organ buds.

MATERIALS AND METHODS

Identifying *Rhou* by gene expression profiling

ARC/s embryos at 4- to 5-somite stages were collected and the anterior intestinal portal was isolated by digestion with trypsin and pancreatin and mechanical dissection. Ectoderm and mesoderm tissues were dissected

[1]Embryology Unit, Children's Medical Research Institute, Westmead, NSW 2145, Australia. [2]Sydney Medical School, University of Sydney, NSW 2006, Australia. [3]The Walter and Eliza Hall Institute of Medical Research, Parkville, Victoria 3050, Australia. [4]Department of Biological Sciences, Macquarie University, NSW 2109, Australia.

*Present address: Westmead Millennium Institute, Westmead, NSW 2145, Australia
†Author for correspondence (ptam@cmri.org.au)

Accepted 9 August 2011

from the head folds and the heart, and combined as the non-endoderm tissues for comparison of gene expression profiles. RNA was extracted from 15-20 pooled samples of endoderm and ectoderm plus mesoderm cells and subjected to two rounds of linear amplification and labelling according to standard methods (Affymetrix). The amplified products were hybridized to Affymetrix mouse MOE430 GeneChips. The experiment was performed twice. RNA amplification labelling, hybridization and scanning were performed by the Australian Genome Research Facility. GC-RMA data normalization and further analysis were performed using GenePattern software.

In situ hybridization

Embryos were collected, fixed in 4% paraformaldehyde (PFA), dehydrated through a methanol series and stored at –20°C. Automated whole-mount in situ hybridization was carried out on an InSituPro machine (AbiMed) using a published protocol (Wilkinson and Nieto, 1993) modified as described previously (Loebel et al., 2004) and stained with BM purple (Roche). Antisense riboprobes were generated from linearized plasmids for *Apom* and *Pax9*, or plasmid inserts amplified with M13 forward and reverse primers for *Rhou* (IMAGE clone 3964150), *Igfbp5* (IMAGE clone 2648602), *Cldn4* (IMAGE clone 876728). A probe for *Pyy* was generated by amplifying a 3′ cDNA fragment by RT-PCR from mouse embryo RNA in two rounds of amplification incorporating a T7 promoter sequence as described (Bildsoe et al., 2009). Primer sequences for *Pyy* riboprobe fragment generation were (5′-3′): *Pyy*F, TGCTCATCTTGC-TTCGGAAGCTGTA; *Pyy*R, TGCGAAATTTGCTTTTTATTTAGGGA; *Pyy*T7R, TAATACGACTCACTATAGGGTGCGAAATTTGCTTTTTAT-TTAGGGA. Digoxygenin-labelled riboprobes were prepared using Ampliscribe Kits (Epicentre).

Mutant mouse strains

Heterozygous *Dkk1* knockout (Mukhopadhyay et al., 2001), *Ctnnb1-bfc* (Nolan et al., 2000) and *Lrp6-Gw* mice (Bogani et al., 2004) were maintained and genotyped as described (Fossat et al., 2011). ROSA-*lacZ* mice were generated by crossing together ROSA26R and CMV-Cre mice and selecting for *lacZ*-expressing offspring.

Generation of shRNA ES cell lines

Oligonucleotides encoding *Rhou*-specific shRNA molecules were designed using the on-line shRNA Explorer tool (www.genelink.com). We used two shRNA constructs (Kunath et al., 2003) containing oligonucleotide sequences against the 3′UTR (*Rhou*-809, *Rhou*-3130; Table 1). In addition, an shRNA construct targeted to the 3′UTR of *Sox17* (Table 1), plus shRNA vector-only and non-targeting shRNA (Sigma Mission Control) were also prepared. The shRNA constructs were electroporated into R1-ES cells and selected for G418 resistance. The degree of knockdown of gene expression for individual clones was assessed by quantitative real-time RT-PCR using primers listed in Table 2.

In vitro differentiation

Two protocols of activin A-directed ES cell differentiation were used. First, ES cells were differentiated as embryoid bodies (EBs) for 2 days followed by 5 days in serum-free media containing 100 ng/ml activin A (Kubo et al., 2004). To test the effects of JNK inhibition, EBs were differentiated in the presence of 10 ng/ml JNK inhibitor 1 (Merck). Second, EBs were generated in differentiation medium for 2.5 days and plated into methylcellulose in IMDM containing 30 ng/ml activin A for 3.5 days followed by plating on matrigel for 4 days. Cells were harvested at the end of the differentiation procedure for RNA extraction.

Generation of chimeric and ES cell-derived embryos

ES cell-derived embryos were generated by injection of ES cells into tetraploid blastocysts or aggregation of ES cells with tetraploid morulae (Nagy et al., 1990). Two-cell embryos, collected from superovulated ARC/S female mice, were electro-fused (CF-150, BLS Hungary) and cultured until the 4-cell stage for aggregation or the blastocyst stage for microinjection. For generating diploid chimeras, ROSA26-*lacZ* males were mated with super-ovulated C57Bl/6 females, embryos collected at the morula stage and cultured until the blastocyst stage for injection. Chimeric blastocysts were transferred to pseudopregnant ARC/s female mice. Embryos were collected 6-7 days after transfer [equivalent to embryonic day (E)8.5-9.5].

Embryo electroporation and culture

DNA constructs encoding GFP-RHOU (Ory et al., 2007), tdTomato-RHOU or shRNAs were introduced into the foreguts of embryos by electroporation as described previously (Khoo et al., 2007). Embryos were electroporated at E8.5 and cultured for 4 hours (GFP-RHOU group) or electroporated at E7.75 (early head-fold stage) and cultured for 24 hours (shRNA group). Embryos were photographed, then fixed in 4% PFA and processed for immunofluorescence. The shRNA constructs were prepared by cloning double stranded oligonucleotides encoding shRNAs (identical to those used in ES cells) into pRNAT-H1.1, which contained a GFP reporter. A non-targeting control was made in the same vector, using the shRNA sequence from the Mission non-targeting control construct (Sigma). A *td-Tomato-RHOU* construct was prepared by excising the GFP from *GFP-RHOU* and replacing it with a PCR product containing the complete open reading frame of *tdTomato*.

Cell culture and transfection

HepG2 human hepatocellular liver carcinoma cells, NIH3T3 cells and NIH3T3-derived lines containing the pLNCX retroviral vector directing constitutive expression of β-galactosidase, *Wnt1*, *Wnt3a*, *Wnt4*, *Wnt5a*, *Wnt7a* or *Wnt11* (Kispert et al., 1998) were maintained in DMEM with 10% foetal calf serum (FCS). For testing the effects of recombinant WNTs, HepG2 cells were cultured for 6 hours in serum-free DMEM containing 200 ng/ml recombinant mouse Wnt3a, Wnt5a, human WNT7A (R&D Systems) or bovine serum albumin (BSA). Cells were transfected with plasmids pEGFP-N2 (control), pCMVSox17-IRES-eGFP (Pfister et al., 2011) or pβcateninS45A-GFP (Johnson et al., 2009) using Fugene6 (Roche) or Lipofectamine LTX (Invitrogen). Transfection with Stealth siRNA against *CTNNB1* (50822) or negative control siRNAs (Invitrogen) was with Lipofectamine RNAiMAX (Invitrogen). Transfected cells were grown for 24 hours and processed for immunofluorescence, or grown for 24 hours (NIH3T3) or 48 hours (HepG2) and harvested for RNA extraction (siRNA transfected cells) or processed for flow sorting to isolate the GFP expressing cells in a FACSVantage cell sorter (plasmid transfection experiments).

RT-PCR and qRT-PCR

RNA was extracted using RNeasy Mini or Micro Kits (Qiagen). First strand cDNA was generated using Superscript III (Invitrogen) and diluted 1:4. RT-PCR was performed using Biomix Taq (Bioline) on a Hybaid multi-block thermocycler for 25-35 cycles. Quantitative real-time RT-PCR (qRT-PCR) was performed using Platinum Taq (Invitrogen) and Sybr Green on a Corbett RotorGene 6000. Primer sequences and annealing temperatures are given in Table 2.

Table 1. Oligonucleotide sequences used to generate shRNA constructs

Name	Sequence
Rhou-809 (sense)	GTACCAAGCTGCAACAGCTCTTTATGGACAAGAGATCCATAAAGAGCTGTTGCAGCTTTTTTTTGGAAAT
Rhou-809 (antisense)	CTAGATTTCCAAAAAAAAGCTGCAACAGCTCTTTATGGATCTCTTGTCCATAAAGAGCTGTTGCAGCTTG
Rhou-3130 (sense)	GTACCAAGCAAACTTCCGAGAACTCCGTCAAGAGAACGGAGTTCTCGGAAGTTTGCTTTTTTTTTGGAAAT
Rhou-3130 (antisense)	CTAGATTTCCAAAAAAAAAGCAAACTTCCGAGAACTCCGTTCTCTTGACGGAGTTCTCGGAAGTTTGCTTG
Sox17-1348 (antisense)	CTAGATTTCCAAAAAGCAGAACCCAGATCTGCACAATCTCTTGTTGTGCAGATCTGGGTTCTGCGGT
Sox17-1348 (antisense)	CTAGATTTCCAAAAAGCAGAACCCAGATCTGCACAATCTCTTGTTGTGCAGATCTGGGTTCTGCGGT

Table 2. Primer sequences for RT-PCR analysis of gene expression

Gene	Species	Forward sequence (5′-3′)	Reverse sequence (5′-3′)	Anneal (°C)	Cycles	Reference
Actb (1)	Mm	CCCCACTCCTAAGAGGAGGATGGTC	CCAGGGAGACCAAAGCCTTCATACA	60	30	
Actb (2)	Mm	AGCACCCTGTGCTGCTCA	GTACGACCAGAGGCATACA	62	Q	
AXIN2	Hs	ATACCGGAGGATGCTGAAGGCTCA	AATCCGGCCTTCATACATCGGGA	62	Q	
Ccnd1	Mm	ATGTGAAGTTCATTTCCAACCCACCC	CAGGCTTGACTCCAGAAGGGCTTC	62	25	
Cldn4	Mm	TATGGTCATCAGCATCATCGTGGGT	GAGTACTTGGCCGAGTAGGGCTTGT	60	35	
CTNNB1	Hs	GTTGGATTGATTCGAAATCTTGCCC	TGAACATCCCGAGCTAGGATGTGAA	62	Q	
Dkk1	Mm	TGCATGAGGCACGCTATGTGC	TTGGACCAGAAGTGTCTTGCA	62	30	
Foxa2	Mm	TGGTCACTGGGGACAAGGGAA	GCAACAACAGCAATAGAGAAC	60	35	
Gapd	Mm	ATGACAACTTTGGCATTGTTGAAGG	CCTGCTTCACCACCTTCTTGATGTC		Q	
Hhex	Mm	TCGAGCTGGAGAAGAAGTTCGAGACT	TCTTGACCCTGCTCACAGGAAGTGT	62	25	
Iapp	Mm	TTGCTGCCTCGGACCACTGAAAG	CACACGTGGCCGTGTTGCACTT	60	30	
Id2	Mm	CAGCACGTCATCGATTACATCTTGGA	TCATTCGACATAAGCTCAGAAGGGAA	62	30	
Kdr	Mm	ACTCCAGCGACGAGGCAGGACTTTT	ATTCTTGGGTCATGGGCATCTTCTCT	60	35	
Krt18	Mm	GATTGACTGTGGAAGTGGATGC	GTTTGCATGGAGTTGCTGGA	60	27	(Tada et al., 2005)
Lefty1	Mm	TGACCGAGGCCGTGAACTTCTG	AGCATCGGGTGCCTTCAGTCACT			
Lhx1	Mm	AAGCAACTGGAGACGTTGAAG	CTGTTTCATCCTTCGCTCCTT	62	25	
Mixl1	Mm	TTCCAGAACCGACGGGCCAAGT	CAGCTCCAATCTCCCAGATCTCCCT	60	35	
Mixl1	Mm	CATGTACCCAGACATCCACTTG	AGGCTTCAAAAACCTAGCTTCA	62	25	
Mug1	Mm	AGTTCTCCATAGATACCACATGCA	ACTCAATGTTGTGCGTAAACTCCA	60	35	
Nkx2-5	Mm	TTTTACCCGGGAGCCTACGGTGA	AGCGACGGTTCTGGAACCAGATCTT	55	35	
Nodal	Mm	TGTGTAGGAGGGTCAAGTTCCAGGTG	ATGCTCAGTGGCTTGGTCTTCACG			
Nrp1	Mm	TTTCTCAGGAAGACTGTGCAAAACCA	TCATGGCTATGATGGTGATCAGGATG	62	30	(Pfister et al., 2011)
Pdx1	Mm	CCGGACATCTCCCCATACGAA	GAGGTCACCGCACAATCTTGC	55	35	(Kubo et al., 2004)
POLR2A	Hs	GCACCACGTCCAATGACAT	GTGCGGCTGCTTCCATAA	62	Q	(Radonic et al., 2004)
Pou5f1	Mm	ATTCCCAACGAGAAGAGTATGAGGCT	TCAACAGCATCACTGAGCTTCTTTCC	60	35	
Pyy	Mm	TGCGCCACTACCTCAACCTGGT	GTGCCCTCTTCTTCTTAAACCAAACATGC	60	30	(Hou et al., 2007)
RHOU	Hs	CCACCGAGTACATCCCTACTGCCTT	CGGCAGTGTCACAGAGTTGGAGTCT	62	Q	
Rhou (1)	Mm	TACATCCCTACGGCCTTCGACAAC	TCTTCAGGCACCGCTTCTCTTT	60	30	
Rhou (2)	Mm	TGTCTGTAGATGGGCGGCCTGT	TTCTGGAAGGATGTGGGGCTCA	62	Q	
Sox17	Mm	CTCTGCCCTGCCGGGATGGCACGGA ATCC	AATGTCGGGGTAGTTGCAATAGTAGACCG CTGA	58	35	
Sox7	Mm	GCCACCTTGCCTGGACTGCAC	ACATGCCCAGTGAGGGTTCC	57	35	
Spred1	Mm	GGAAGATCGATGACAAGAAGTTTGGC	TGGTAACAACTGTCTCTTGCTGGAAA	62	30	
Spry2	Mm	TCAGGACTGGATTTATTTGCACATCG	TACCTGCTGGGTAAGGGCATCTCTT	62	30	
T	Mm	AACGGGCTGGGAGCTCAGTTCTT	TAAAGTAGGACAGGGGGTGGACGAAT	60	30	
Ttr	Mm	AGTCCTGGATGCTGTCCGAG	TTCCTGAGCTGCTAACACGG	60	35	(Kubo et al., 2004)
Wnt1	Mm	CTTCGAGAAATCGCCCAACTTCT	ATCGCTATGAACCCTGGGACTGTG	60	35	
Wnt5a	Mm	TCCTATGAGAGCGCACGCAT	CAGCTTGCCCCGGCTGTTGA	62	30	

Q, primers used for qRT-PCR; others were used for RT-PCR with the indicated number of cycles.
Mm, *Mus musculus*; Hs, *Homo sapiens*.
References are given for previously published primer sequences.

Immunofluorescence analysis

Embryos and embryoid bodies were fixed overnight at 4°C in 4% PFA, permeated with sucrose/PBS and infiltrated with a 1:2 mixture of 30% sucrose in PBS and O.C.T. compound, frozen, sectioned (7 μm) and stored at –80°C. Transfected HepG2 cells grown on coverslips were fixed in 4% PFA for 5 minutes and washed in PBS before phalloidin staining. The following primary antibodies were used: rabbit anti-ZO-1 (Invitrogen 40-2200, 6 μg/ml); rat anti-E-cadherin (Invitrogen 13-1900, 6 μg/ml); rat anti-fibronectin (Abcam ab23750, 5 μg/ml); rabbit-anti GFP (Invitrogen A11122) mouse anti-GFP (ABCAM), rabbit anti-dsRed (Clontech) and mouse anti-acetylated α-tubulin (Abcam ab24610, 4 μg/ml). Secondary antibodies used were: Cy2 donkey anti-mouse IgG (Jackson ImmunoResearch, 4.2 μg/ml), Alexa Fluor 633-conjugated goat anti-rabbit IgG (Invitrogen, 10 μg/ml) and Alexa Fluor 488-conjugated goat anti-rat IgG (Invitrogen, 6 μg/ml). F-actin was detected with Alexa Fluor 546-conjugated phalloidin (Invitrogen).

Immunofluorescence was imaged with a Leica TCS SP2 confocal microscope using a 100× objective. Pixel intensity and cellular dimensions were measured on unmodified images using ImageJ. Contrast and levels were adjusted for display with Adobe Photoshop.

Transmission electron microscopy (TEM)

PFA-fixed embryos were embedded in epoxy resin sectioned and viewed with a Philips CM10 transmission electron microscope (Miranda-Saksena et al., 2000).

Whole-mount staining for β-galactosidase activity

Embryos were collected in PB1 medium (Kinder et al., 2000), rinsed in PBS and fixed for at least 2 hours in glutaraldehyde solution (0.02% Igepal CA630, 0.01% sodium deoxycholate, 0.2% glutaraldehyde, 5 mM EGTA, 2 mM $MgCl_2$), washed in Lac Z washing buffer (Watson et al., 2008) briefly before being incubated in Lac Z staining solution (Watson et al., 2008) at 37°C for colour development. The embryos were then washed in PBS and fixed in 4% PFA.

Histology

Fixed embryos were processed for wax histology by dehydrating through a graded ethanol series and embedding in paraffin wax. Embedded specimens were sectioned, transferred to SuperFrost slides (Menzel) and stained with Nuclear Fast Red or Haematoxylin and Eosin.

RESULTS

Rhou is expressed in the foregut endoderm

Microarray analysis was carried out on RNA extracted from dissected foregut endoderm and combined headfold and heart tissues (ectoderm and mesoderm; see Fig. S1A,B in the supplementary material). Differential expression analysis revealed that the foregut endoderm samples were enriched with genes with

known endoderm-specific expression, confirming the efficacy of the isolation strategy (see Fig. S1C in the supplementary material). To identify Rho-related small GTPases in epithelial tissues, we searched for genes encoding Rho GTPases that displayed preferential expression in the endoderm. One such gene, *Rhou*, was found to be strongly upregulated in the endoderm (see Fig. S1C in the supplementary material).

Rhou expression was first detected by in situ hybridization in the anterior DE of early-somite embryos. At the 3-somite stage, *Rhou* expression was strongest in the rim of the foregut pocket (Fig. 1A,B), where the liver progenitors reside (Tremblay and Zaret, 2005). At E8.5 (8 somites), *Rhou* was expressed throughout the foregut except the regions anterior to the first branchial arch and the ventral lip of the anterior intestinal portal (AIP) (Fig. 1C,Ci-iii). *Rhou* expression was strong in the columnar epithelium on the lateral wall and the floor of the foregut but weak in the thin squamous epithelium of the roof (Fig. 1Ci,ii). Unlike in *Xenopus* embryos (Fort et al., 2011), *Rhou* expression was not detected in migrating cranial neural crest cells. At E9.5, *Rhou* was expressed in the pharyngeal pouches (Fig. 1D,Di) and the endoderm on the lateral wall of the caudal segment of the AIP. *Rhou* was weakly expressed in the thickened epithelium on the floor of the foregut where the thyroid primordium emerges (Fig. 1Di) and was not detected in the liver bud (Fig. 1Dii). By E10.0, *Rhou* expression was weak in the foregut (not shown). The timing and domain of expression of *Rhou* in the foregut endoderm suggest an association with the development or maintenance of the columnar epithelium of the foregut endoderm.

Rhou is upregulated in response to increased canonical WNT signalling

Rhou was originally identified by its upregulation by Wnt1 in cultured cells (Tao et al., 2001) and might, therefore, be involved in mediating the effects of Wnt signalling on endoderm development (Hansson et al., 2009; Lickert et al., 2005). To examine the effects of elevated Wnt signalling activity in embryos we compared *Rhou* expression in wild-type E8.5 mouse embryos with embryos harbouring mutations that enhance canonical Wnt signalling activity: the Batface (*Bfc*) allele of *Ctnnb1* and the Gwazi (*Gw*) allele of *Lrp6* (Fossat et al., 2011). Upregulation of *Rhou* was observed in $Ctnnb1b^{bfc/bfc}$ and $Lrp6^{Gw/+}$ embryos (Fig. 2A,B). *Rhou* expression in $Lrp6^{Gw/Gw}$ embryos was variable, consistent with the incomplete penetrance of the mutant phenotype (Fossat et al., 2011). We also observed increased *Rhou* expression in $Dkk1^{+/-}$ and $Dkk1^{-/-}$ embryos by qRT-PCR, and in the foregut and adjacent tissues of $Dkk1^{-/-}$ embryos by in situ hybridization (Fig. 2C-G).

To explore the regulation of *Rhou* by Wnt signalling further, we examined the effects of expressing various Wnt factors on Rhou expression in NIH-3T3 cells. Rhou was induced most strongly by Wnt1 and Wnt3a and was above basal levels in the Wnt7a-expressing cells (Fig. 2H). Expression of Dkk1, a canonical Wnt target, was strongly enhanced in cell lines expressing Wnt1 and Wnt7a (Fig. 2H). These ligands primarily activate canonical Wnt pathways. Consistent with the involvement of canonical Wnt signalling, transfection of NIH3T3 cells with a construct encoding phosphorylation-resistant β-catenin point mutant (S45A) resulted in an approximately threefold upregulation of Rhou over the control transfected cells (Fig. 2I).

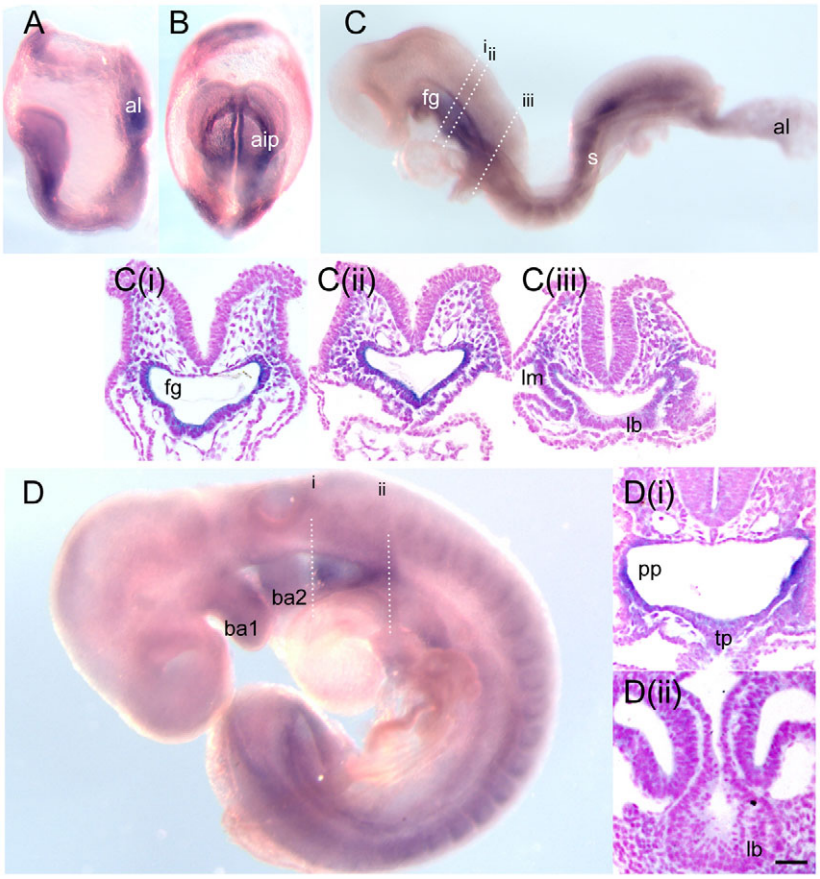

Fig. 1. *Rhou* expression in the foregut endoderm of post-implantation mouse embryos. (**A**,**B**) At E8.0 (3-somite stage), *Rhou* is expressed strongly around the rim of the anterior intestinal portal (aip) and allantois (al). (**C**) At E8.5 (8-somite stage), *Rhou* is expressed on the lateral and the ventral wall of the foregut (fg) but is downregulated in the epithelium that will contribute to the liver bud (lb). (**Ci-Ciii**) Sections through the planes indicated in C. (**D**) At E9.5, *Rhou* is expressed in the endoderm of the pharyngeal pouches and the lateral wall of the upper foregut but is downregulated in the liver bud (lb) and the ventral endoderm where the thyroid primordium (tp) forms. (**Di**,**Dii**) Sections through the planes indicated in D. Scale bar: 100 μm. ba1, ba2: first and second branchial arch; lm, lateral mesoderm; pp, pharyngeal pouch; s, somite.

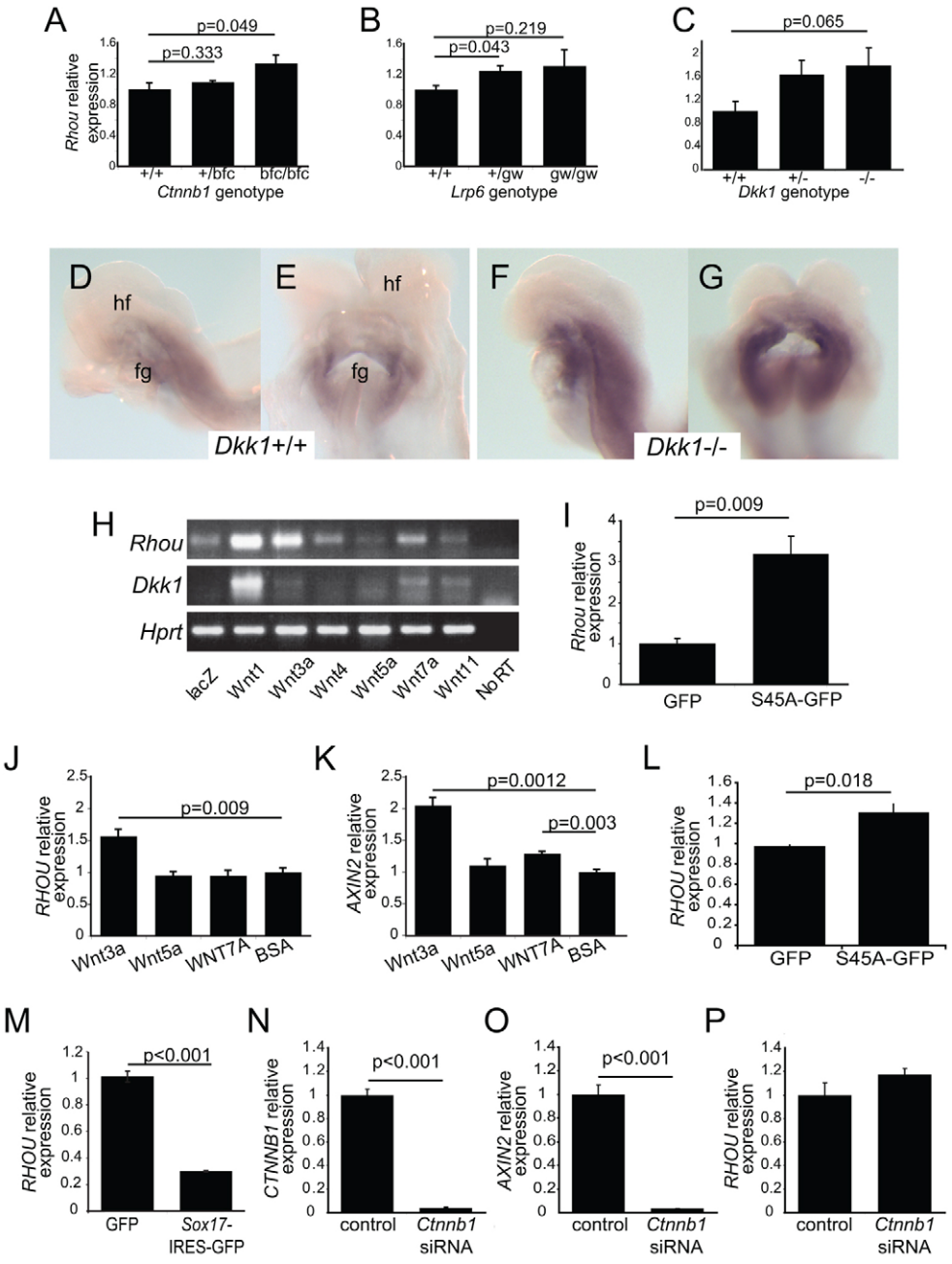

Fig. 2. Regulation of *Rhou* by canonical Wnt signalling activity. (**A-C**) Quantitative RT-PCR analysis of *Rhou* expression in of homozygous *Bfc*, *Gw* and *Dkk1* mutant E8.5 mouse embryos compared with heterozygous and wild-type embryos. *n*=4 for *Dkk1*, *n*=3 for others. (**D-G**) In situ hybridization to wild-type (D,E; *n*=2) and *Dkk1*$^{-/-}$ (F,G; *n*=2) embryos, revealing upregulation of *Rhou* in the mutants. D,F: lateral view; E,G: ventral view. fg, foregut; hf, headfold. (**H**) RT-PCR analysis revealing upregulation of *Rhou* in NIH3T3 cells expressing *Wnt1*, *Wnt3* and *Wnt7a*. Expression of *Dkk1*, a Wnt target gene, is shown for comparison. *Hprt*, loading control; no-RT and *lacZ*, no reverse transcriptase and *lacZ* for background control. (**I**) Quantitative RT-PCR analysis of NIH3T3 cells transiently transfected with either a GFP-expressing plasmid, or a plasmid encoding a point mutant of β-catenin conferring constitutive transcriptional activity (S45A-GFP). (**J**,**K**) Quantitative RT-PCR analysis of *RHOU* (J) and *AXIN2* (K) expression in HepG2 cells treated with recombinant Wnt3a, Wnt5a or WNT7A, with BSA as the control. (**L**) Expression of *RHOU* in HepG2 cells transfected with β-catenin S45A-GFP. (**M**) Expression of *RHOU* in HepG2 cells transfected with the plasmid coding for GFP or Sox17-IRES-GFP. (**N-P**) Expression of *CTNNB1* (N), *AXIN2* (O) and *RHOU* (P) in cells transfected with control or *CTNNB1*-specific siRNA. Reference genes: *Actnb* for I; *POLR2A* for J-P. *P*-values of two-tailed *t*-tests for pairs of treatment groups are shown. Error bars represent s.e.m.

To test the response of *RHOU* to WNT signalling in cells that are more closely related to endoderm, HepG2 cells were cultured with recombinant mouse Wnt3a, Wnt5a and human WNT7A. *RHOU* was only upregulated by Wnt3a, whereas *AXIN2*, a canonical WNT target, was significantly upregulated by Wnt3a and WNT7A (Fig. 2J,K). Consistent with this, transfection of HepG2 cells with β-catenin-S45A-GFP also resulted in upregulation of *RHOU* (Fig. 2L). Sox17, a transcription factor crucial for DE development (Kanai-Azuma et al., 2002; Pfister et al., 2011) inhibits the transcriptional response of *Rhou* to canonical Wnt signalling (Jia et al., 2010; Zorn et al., 1999). Transfection of a Sox17-IRES-GFP expression construct reduced *RHOU* expression to one-third of the GFP-only control (Fig. 2M). However, knockdown of β-catenin did not result in downregulation of *RHOU* (Fig. 2N-P), suggesting that Sox17 regulates Rhou expression via β-catenin-independent means in HepG2 cells and that although the level of canonical WNT signalling activity can influence RHOU expression, *Rhou* is not a direct β-catenin target.

Reduced Rhou activity impairs endoderm differentiation of ES cells

To investigate the requirement for Rhou in the differentiation of endoderm lineages, we generated Rhou knockdown (KD) ES cell lines. Two KD ES cell lines, *Rhou*809-9 and *Rhou*3130-3, harbouring different shRNAs that displayed 71% and 59% reduction in *Rhou* expression, respectively, compared with vector controls as measured by qRT-PCR were selected for this study.

In a preliminary experiment, in which a vector control and one KD ES cell line (*Rhou*3130-3) were differentiated as EBs for 15 days, the *Rhou* KD line showed a delayed and less robust upregulation of genes associated with mesendoderm progenitors,

endoderm and mesoderm lineages [*T*, *Mixl1*, *Flk1* (*Kdr* – Mouse Genome Informatics), *Mug1*], but maintained prolonged expression of the pluripotency marker *Pou5f1* (see Fig. S2A,C,D in the supplementary material).

Culturing ES cells in the presence of activin A can enhance the differentiation of endodermal derivatives (see Fig. S2B,D in the supplementary material) (D'Amour et al., 2005; Kubo et al., 2004; Tada et al., 2005). To test whether knockdown of *Rhou* in ES cells impacts the differentiation of endodermal lineage in response to activin induction, we examined the expression of endoderm markers by RT-PCR (see Fig. S3A in the supplementary material). The strongest differences between KD and control cell lines were observed for genes that mark the hepatic (*Hhex*, *Ttr*, *Mug1*) or pancreatic lineages (*Pdx1*, *Iapp*). In several cases, the relative degree of downregulation of markers (notably *Foxa2*, *Pdx1* and *Ttr*) in the KD cells correlated with the level of *Rhou* knockdown in the differentiated cells. *Ttr* is a target of AP1 transcription factor complexes, which contain the transcription factor c-Jun (Qian et al., 1995) and RHOU has been shown to influence AP-1 activity that is downstream of JNK (Zhang et al., 2011). Differentiation of EBs lacking JNK1 and JNK2 activity (Xu and Davis, 2010) or EBs in the presence of JNK inhibitor reduced the expression of some endodermal lineage markers (see Fig. S4 in the supplementary material). To study further the RHOU-JNK-AP1/c-Jun cascade, we examined other targets of AP1/c-Jun and found that *Nrp1*, *Wnt5a* and *Dkk1* were downregulated in *Rhou* KD cells (see Fig. S3B in the supplementary material). In contrast to *Dkk1*, another Wnt target gene, *Ccnd1*, did not change its expression in KD cells. *Hhex* (see Fig. S3A in the supplementary material), a direct target of bone morphogenetic protein (Bmp) signalling was downregulated in *Rhou* KD EBs, but another Bmp target, *Id2*, was not (see Fig. S3B in the supplementary material). There was no change in the expression of targets of nodal signalling (*Lefty1*, *Nodal*) or fibroblast growth factor (Fgf) signalling (*Spry2*, *Spred*; see Fig. S3B in the supplementary material). Our data suggest that *Rhou* knockdown affects the JNK-AP1/c-Jun activity and some aspects of the Wnt and Bmp signalling cascades.

To test further the differentiation potency of the *Rhou*-KD ES cells, we cultured EBs in a lower concentration of activin A (30 ng/ml) on matrigel, which promotes both mesoderm and endoderm differentiation (Kubo et al., 2004). *Rhou*-deficient ES cells upregulated genes associated with cardiac mesoderm more robustly than did control cells (see Fig. S5 in the supplementary material). KD cells differentiated under these conditions generated more colonies (percentage of total number scored) with rhythmic beating activity than did control cells (control 1: 27.8±28; *Rhou*809-9: 97.6±2.4; *Rhou*3130-3: 84.2±15.9; mean ± s.e.m.), suggesting an enhancement of mesoderm differentiation. Overall, differentiation studies performed under two different conditions showed that *Rhou* KD adversely affects the ability of ES cells to differentiate into endoderm derivatives but facilitates mesoderm differentiation.

Defective foregut endoderm development in *Rhou* KD embryos

To analyse the role of Rhou in the development of the foregut endoderm in vivo, we studied the phenotype of embryos derived from *Rhou* KD ES cells by tetraploid complementation (Kunath et al., 2003; Nagy et al., 1990). To verify the efficacy of our techniques, we established that: (1) tetraploid embryos implanted but failed to develop; (2) embryos that were generated by injection of diploid ES cells harbouring a non-targeting shRNA construct into tetraploid blastocysts developed into morphologically normal embryos at E8.5 and E9.5; (3) in morphologically normal embryos generated from tetraploid hosts and wild-type ES cells, the ES cell contribution was very high; (4) ES-cell derived *Sox17*-knockdown embryos phenocopied *Sox17*-null mutant embryos; and (5) the tetraploid host cells did not contribute significantly to the foregut of the ES-derived chimera (see Fig. S6 in the supplementary material). The efficiency of generation of embryos was similar for the control and two KD cell lines (see Table S1 in the supplementary material).

Rhou expression was markedly reduced in KD embryos (Fig. 3A-C), indicating the shRNA knockdown was sustained during post-implantation development. Both lines of KD embryos displayed abnormalities, including a failure to turn, closely

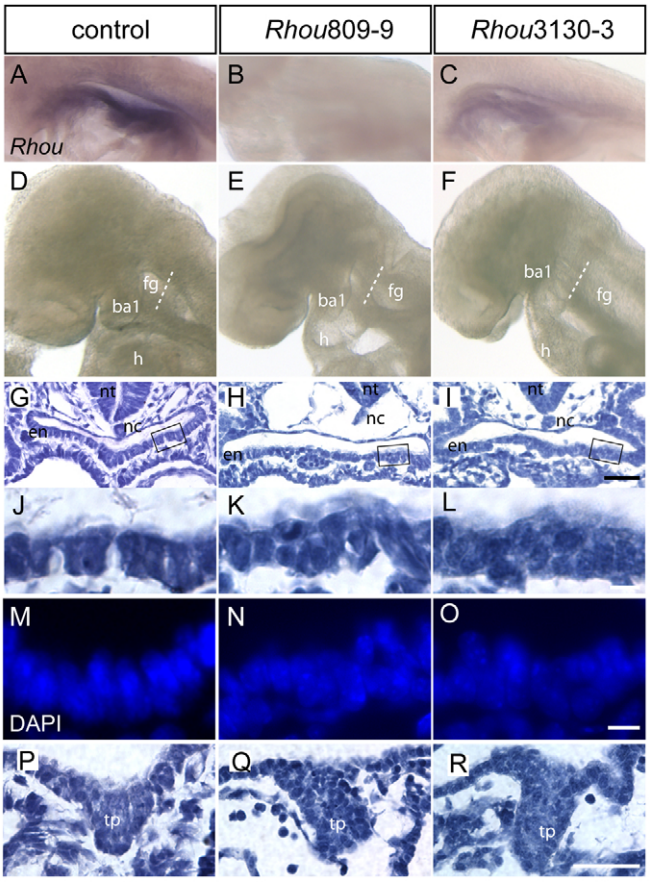

Fig. 3. Altered epithelial architecture in the foregut endoderm of mouse embryos derived from *Rhou*-knockdown ES cells. (**A-C**) In situ hybridization of E8.5 embryos harbouring control (A), *Rhou*809-9 (B) or *Rhou*3130-3 (C) shRNA constructs, showing reduced *Rhou* expression in knockdown embryos. (**D-F**) Lateral views of the head region of embryos derived from control (D), *Rhou*809-9 (E) and *Rhou*3130-3 (F) ES cell lines, showing the collapsed foregut of the knockdown embryos. (**G-L**) Sections through the foregut of control (G) and knockdown (H,I) embryos at the planes (dotted lines) indicated in the panel immediately above. J-L show magnified views of the boxed areas of the epithelium in G-I, respectively. (**M-O**) DAPI staining revealing the irregular arrangement of the nuclei in the epithelium of the foregut. (**P-R**) Sections of control (P) and knockdown (Q,R) embryos showing the abnormal shape and enlarged size of the thyroid primordium in the *Rhou*-deficient embryos. ba1, first branchial arch; en, endoderm; fg, foregut; h, heart; nc, notochord; nt, neural tube; tp, thyroid primordium. Scale bars: 100 μm for G-I; 10 μm for J-O; 100 μm for P-R.

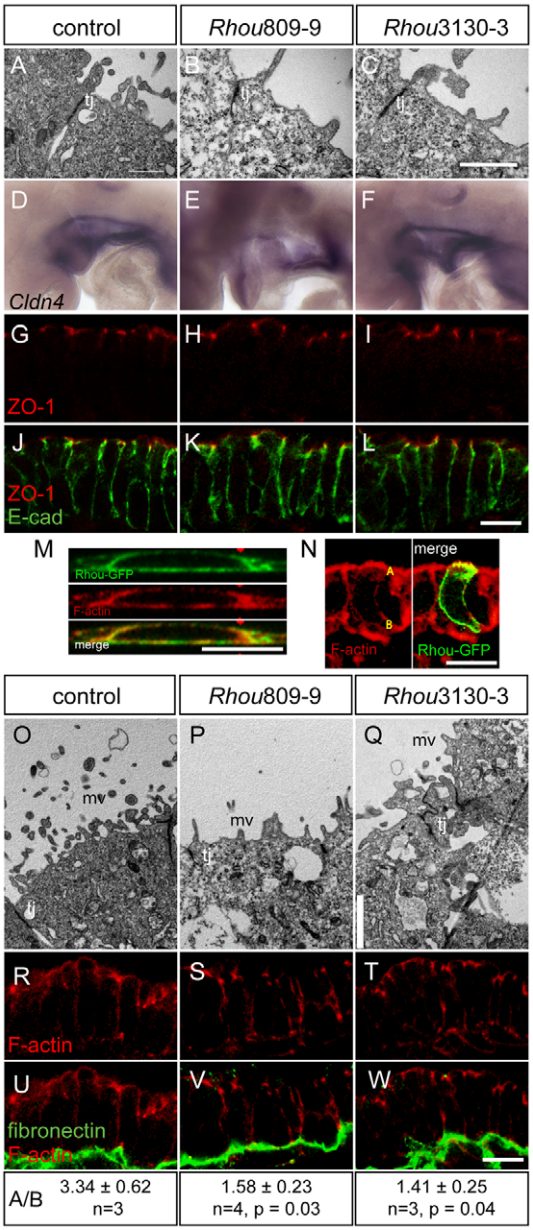

Fig. 4. Impact of *Rhou* deficiency on cell junctions and F-actin distribution. (**A-C**) Ultrastructure of the apical region of the foregut endoderm cells of control (A), *Rhou*809-9 (B) and *Rhou*3130-3 (C) knockdown embryos, showing formation of tight junctions (tj) but depletion of cytoplasmic inclusions, such as electron dense granules and ribosomal particles, and vacuolation of the cytoplasm in the *Rhou*-deficient endoderm cells. (**D-F**) *Cldn4* expression revealed by whole-mount in situ hybridization in control (D) and knockdown (E,F) embryos. (**G-I**) Confocal immunofluorescence images of the foregut epithelium of control (G) and knockdown (H,I) embryos showing the presence of ZO-1, a marker of apical tight junctions. (**J-L**) Merged images of ZO-1 (red) and E-cadherin (green) immunofluorescence. (**M**) Colocalization of GFP-RHOU and F-actin (stained by phalloidin) in the sub-membrane domain of the transfected HepG2 cell. The images are *xz* reconstructions from serial confocal images in the *xy*-plane (coverslip surface is at the bottom of the images). (**N**) Colocalization (yellow) of GFP-RHOU and F-actin in apical region of the foregut endoderm cells of E8.5 embryo. A, apical aspect; B, basal aspect. (**O-Q**) The apical surface of endoderm cells of *Rhou*-deficient embryos (P,Q) are decorated by fewer and shorter microvilli than that of the control embryo (O). (**R-T**) Confocal images showing the accumulation of F-actin in the sub-apical cortical domain of the foregut endoderm cells of the control embryo (R) that contrasts with the scattered distribution of F-actin in the endoderm cells of the Rhou-deficient embryos (S,T). (**U-W**) Merged confocal images showing the scattered distribution of F-actin in the apical and lateral regions of the *Rhou*-deficient endoderm cells. Fibronectin marks the basal side of the epithelium. A/B indicates measurement of the relative pixel intensity of phalloidin-stained materials at the apical (A) and basal (B) aspects of the foregut endoderm cells of the control and *Rhou*-deficient embryos. Data are shown as mean ± s.e.m. and tested for significant differences by two-tailed *t*-test. Scale bar: 1 μm for A-C; 10 μm for G-N,R-W; 2 μm for O-Q. *n*=number of embryos. Measurements were taken from three optical slices through sections of each of the 10-15 cells analysed per embryo.

packed somites and a bulbous allantois that failed to connect with the chorion (see Fig. S6I-N in the supplementary material). The foregut of KD embryos was dorsoventrally flattened (in 22/26 *Rhou*809-9 and 28/33 *Rhou*3130-3 embryos; Fig. 3E,F). By contrast, majority of control embryos (25/28) showed a normal-shaped foregut (Fig. 3D). These phenotypes were not specific to the chosen cell lines. Embryos generated from one additional line each that harboured the *Rhou*809 or *Rhou*3130 shRNA construct also displayed similar phenotypes (see Fig. S7A,B in the supplementary material).

Histological examination of *Rhou* KD embryos revealed that the ventral and lateral endoderm epithelium in the foregut was irregular in thickness. In the most severely affected regions, cells appeared to pile up on each other, revealed by the positions of the nuclei and contrasting with the orderly cell organization in control embryos (Fig. 3G-O). The apical-basal positions of nuclei in the endoderm cell did not differ between control and KD embryos. KD endoderm cells were shorter in height and the nuclei were rounder (see Fig. S8 in the supplementary material). In both control and *Rhou* KD embryos, a multilayered thyroid primordium emerged from the floor of the foregut. However, the primordium of the *Rhou* KD embryos contained more cells, had an abnormal shape and elongated further away from the floor of the gut (Fig. 3P-R). These findings show that *Rhou* activity is required for proper epithelial morphogenesis of the endoderm.

Cell junctions are maintained in *Rhou* KD endoderm

The disruption of the columnar epithelial architecture of the foregut endoderm in *Rhou* KD embryos suggests an inability of the endoderm cells to maintain proper physical connection with the neighbouring cells. To address this, we examined the organization of tight and adherens junctions. When viewed by TEM, electron-dense tight junctions were found in the sub-apical lateral cell membranes of the foregut endoderm of control and *Rhou* KD embryos (Fig. 4A-C). Consistent with this, *Cldn4* was expressed in both control and KD foregut endoderm (Fig. 4D-F) and ZO-1 (Tjp1 – Mouse Genome Informatics) was also properly localized (Fig. 4G-L). E-cadherin distribution in the adherens junctions was similar in control and KD embryos (Fig. 4J-L). These findings indicate that *Rhou*-deficient foregut endoderm cells can maintain the proper intercellular junctions required for epithelial organization.

Altered distribution of apical F-actin in the endoderm of *Rhou* KD embryos

TEM examination of the DE of KD embryos revealed a paucity of microvilli at the apical cell surfaces of endoderm cells (Fig. 4O-Q). Because microvilli contain a core of actin microfilaments (Vicente-Manzanares and Sanchez-Madrid, 2000), we tested whether Rhou and F-actin could potentially interact by examining their localization. A GFP-RHOU fusion protein (Ory et al., 2007) expressed in HepG2 cells was colocalized with F-actin in the cortical cytoplasm (Fig. 4M), and was preferentially localized in the F-actin-enriched apical domain of the DE cells in the foregut (Fig. 4N). We then examined the distribution of F-actin in the DE of KD embryos derived from the two KD cell lines. In both types of KD embryos, there was a marked reduction in F-actin in the apical region of the endoderm cell (Fig. 4R-W; see Fig. S9A-C in the supplementary material). This observation was supported by the reduction in the mean apical:basal ratio of pixel intensity of phalloidin staining in the endoderm cells of KD embryos. In addition, acetylated α-tubulin was dispersed away from the apical region of the KD endoderm cells (see Fig. S9D,E in the supplementary material). These findings show that less F-actin and acetylated α-tubulin is localized to the apical domain of Rhou-deficient cells.

We also examined F-actin, ZO-1 and E-cadherin localization in the endoderm-like cells on the surface of EBs cultured with activin A (see Fig. S10 in the supplementary material). We observed reduced content of apical F-actin in the superficial cells and widespread ZO-1 localization to deeper cells in the *Rhou* KD EBs. Knockdown of *Rhou* activity, therefore, affects the localization of the F-actin and tight junctions in the endoderm-like cells in the EBs.

Rhou knockdown affects cellular position in the epithelium

To test whether the impact of *Rhou* deficiency was cell-autonomous, individual to small groups of cells in the foregut endoderm were subject to focal electroporation of *Rhou* shRNA constructs (*Rhou*809GFP and *Rhou*3130GFP) and a non-targeting control construct (NTC-GFP), all with a GFP reporter to enable identification of the electroporated cells. After 24 hours of culture, the majority (21/26) of NTC-GFP-expressing endoderm cells of the control group embryos retained their proper position in the epithelium and maintained connection with the apical surface of the epithelium (Fig. 5A-B′). By contrast, endoderm cells harbouring shRNAs were often sequestered to the basal side of the epithelium (*Rhou*809GFP: 13/26 cells, χ^2=5.43, P<0.025; *Rhou*3130GFP: 27/52 cells, χ^2=11.8, P<0.001; both significantly

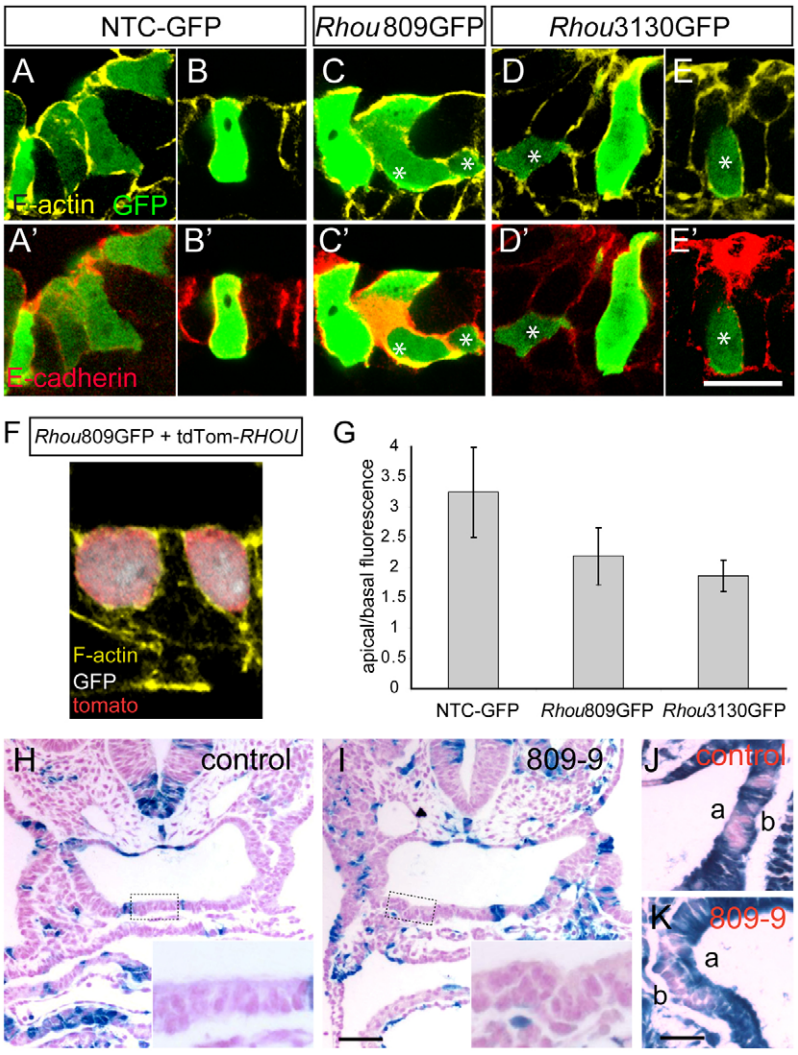

Fig. 5. Effects of *Rhou* knockdown on cell position and F-actin distribution in the foregut endoderm. (**A-E′**) Merged images of phalloidin staining and E-cadherin (A′-E′) with GFP immunofluorescence. (A-B′) Electroporation of a non-targeting control shRNA construct (NTC-GFP). (C-E′) Expression of *Rhou*809GFP (C,C′) *Rhou*3130GFP (D-E′) results in the distortion of cell shape or the retraction of the cells (asterisks) from the apical surface of the epithelium. Images are oriented with apical surface towards the top. (**F**) Co-expression (grey) of *Rhou*809GFP and td-Tomato-*RHOU* constructs counteracted the effect of *Rhou* knockdown on apical positioning. (**G**) Measurement of pixel intensity of phalloidin-stained materials in the apical and basal aspects of control and shRNA-expressing cells that still maintained their full apical-basal dimension in the epithelium. Control, *n*=19; *Rhou*809GFP, *n*=14; shRNA2, *n*=15; *n*=number of cells. Error bars represent s.e.m. (**H-K**) Diploid chimeras generated from ROSA-*lacZ* × ARC/S host embryos and control (H,J) or Rhou809-9 (I,K) ES cells, where the ES cell contribution (unstained cells) is high (H,I) or low (J,K). Insets in H and I are magnified views of the boxed areas. Scale bars: 10 μm for A-E′; 100 μm for H,I; 200 μm for J,K. a, apical; b, basal.

more than the control: 5/26 cells; Fig. 5C-E′). The cells that were sequestered basally remained within the E-cadherin-expressing epithelium (Fig. 5A′-E′). The yielding of apical positioning by *Rhou*809GFP-expressing cells was counteracted by co-electroporation of a construct encoding tdTomato-RHOU (Fig. 5F), resulting in only 4/22 cells being sequestered below apical surface, which is comparable to the control. Measurement of apical:basal ratios of phalloidin fluorescence revealed that individual KD endoderm cells that were able to maintained an apical presence already displayed a reduction in apical F-actin content (Fig. 5G). In diploid chimeras generated from *lacZ*-expressing host embryos and unlabelled *Rhou*809-9 ES cells, *Rhou* KD cells were able to colonize the endoderm extensively (Fig. 5H,I). In these diploid chimeras, the endoderm occupied by the KD (*lacZ*-negative) cells displayed an irregular appearance similar to that of the endoderm of the ES-tetraploid chimeras (Fig. 5H,I insets). Where the ES cell contribution was low, clusters of *Rhou* KD (*lacZ*-negative) cells tended to be localized basally in the epithelium (Fig. 5J,K). These data show that *Rhou* knockdown has little effect on endoderm potency of the ES cells but impairs ability of endoderm cells to maintain their proper position within the epithelium and this is associated with the disruption in F-actin distribution.

Rhou knockdown disrupts endoderm differentiation

To establish whether the disruption of epithelial morphogenesis by *Rhou* knockdown affects DE differentiation in the embryo, endoderm marker expression was analysed by in situ hybridization. Because *Rhou* KD embryos were malformed by E9.5 and few survived beyond E10 (see Fig. S6M,N in the supplementary material), the present study focussed on E8.5-9.5 embryos. *Igfbp5* and *Pax9*, which were expressed in the foregut in control embryos (Fig. 6A,D), were markedly reduced in KD embryos (Fig. 6B,C,E,F). *Pyy* (Hou et al., 2007), which was expressed in the posterior-ventral foregut endoderm and at the prospective site of the pancreatic primordium in control embryos (Fig. 6G), was reduced to small patches (Fig. 6H,I) or nearly absent (Fig. 6H-K) in *Rhou* KD embryos (and in embryos generated from two other KD cell lines, see Fig. S7C-E in the supplementary material). *Apom*, which was expressed in the liver bud of control embryos, (Fig. 6L) was weakly expressed in KD embryos (Fig. 6M,N). *Apom*-expressing structures reminiscent of the liver bud were formed in the *Rhou*3103-3 KD embryos, whereas in the *Rhou*809-9 KD embryos, the *Apom*-expressing cells were confined to a thin layer of cells in the bud-like structure (Fig. 6L-N, insets). Disruption of the epithelial morphology of the endoderm progenitors during early development of anterior intestinal portal therefore has an adverse impact on liver cell differentiation.

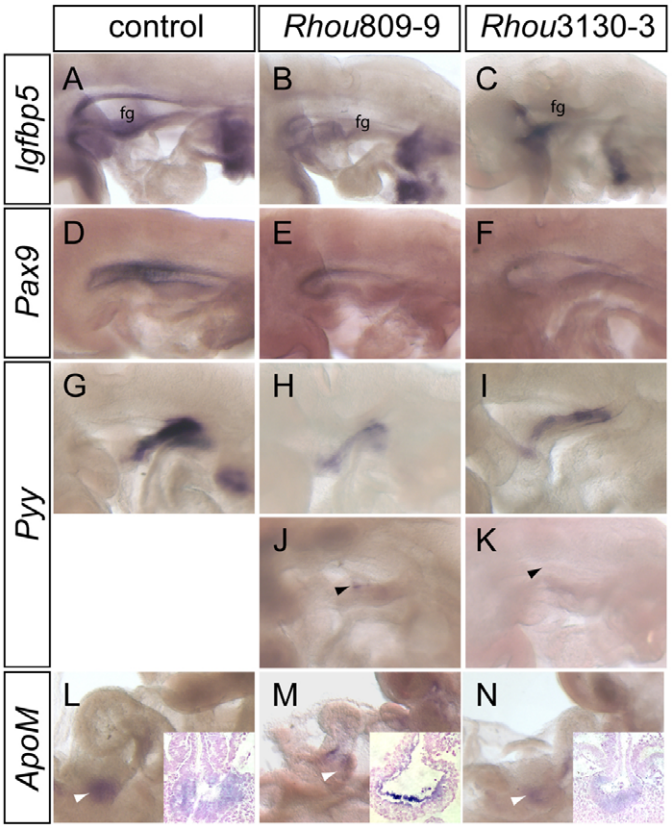

Fig. 6. *Rhou* deficiency impacts on endoderm differentiation in the foregut (fg). (**A-N**) Whole-mount in situ hybridization of embryos derived from control (A,D,G,L), *Rhou*809-9 (B,E,H,J,M) and *Rhou*3130-3 (C,F,I,K,N) ES cells showing representative expression of *Igfbp5* (A, 3/3 control; B,C, weak expression in 2/3 *Rhou*809-9 embryos and 3/3 *Rhou*3130-3 embryos), *Pax9* (D-F, 3/3 control; 4/4 *Rhou*809-9 embryos, 2/3 *Rhou*3130-3 embryos), *Pyy* (G, 4/4 control; H-I, weak expression in 2/3 *Rhou*809-9 embryos and 4/5 *Rhou*3130-3 embryos; J-K, little or no expression in 1/3 *Rhou*809-9 embryos and 1/5 *Rhou*3130-3 embryos) and *Apom* (L, 3/3 control; M,N, weak expression in 2/3 *Rhou*809-9 embryos and 2/3 *Rhou*3130-3 embryos). Insets in L-N show transverse sections of the liver bud. Black arrowheads point to small regions of residual *Pyy* expression. White arrowheads indicate *Apom*-expressing liver bud.

DISCUSSION

In this study, we show that depletion of *Rhou* leads to altered F-actin distribution and disrupts epithelial morphogenesis of the endoderm. Reduced *Rhou* activity affects cellular morphology and cytoskeletal organization in cultured cells (Aspenstrom et al., 2004; Brady et al., 2009; Saras et al., 2004). Of particular note, *Rhou* knockdown in MDCK cells disrupts epithelial cyst formation in a three-dimensional matrix (Brady et al., 2009). These findings suggest that *Rhou* activity is essential for the maintenance of cellular and tissue architecture.

Between E8.0 and E8.5 the lateral and rostral parts of the anterior definitive endoderm converge in the midline to form the foregut pocket (Franklin et al., 2008; Tremblay and Zaret, 2005). Concurrently, the endoderm in the peripheral prospective foregut pocket changes from squamous to columnar morphology and F-actin accumulates apically (Fig. 7A). *Rhou* expression encompasses the sites where liver progenitor cells are localized (Tremblay and Zaret, 2005). After the anterior intestinal portal is formed, *Rhou* expression is maintained in the ventral and lateral foregut endoderm. Rhou is not expressed in the dorsal foregut endoderm, which remains squamous and lacks apical-basal F-actin polarization, and also not in the emerging liver primordium where the epithelium has transformed into a multilayered cell sheet (Fig. 7A). F-actin is a key structural component of the cytoskeleton and is crucial for the maintenance of intercellular junctions, microvilli and cell-substrate interactions (Harris et al., 2009; Ofek et al., 2009). The function of Rhou in maintaining epithelial morphology and F-actin and α-tubulin distribution is probably cell-autonomous as only cells with *Rhou* KD lose their ability to maintain their apical position in the epithelium and the phenotypic changes do not affect the neighbouring cells (Fig. 7B). F-actin is also responsible

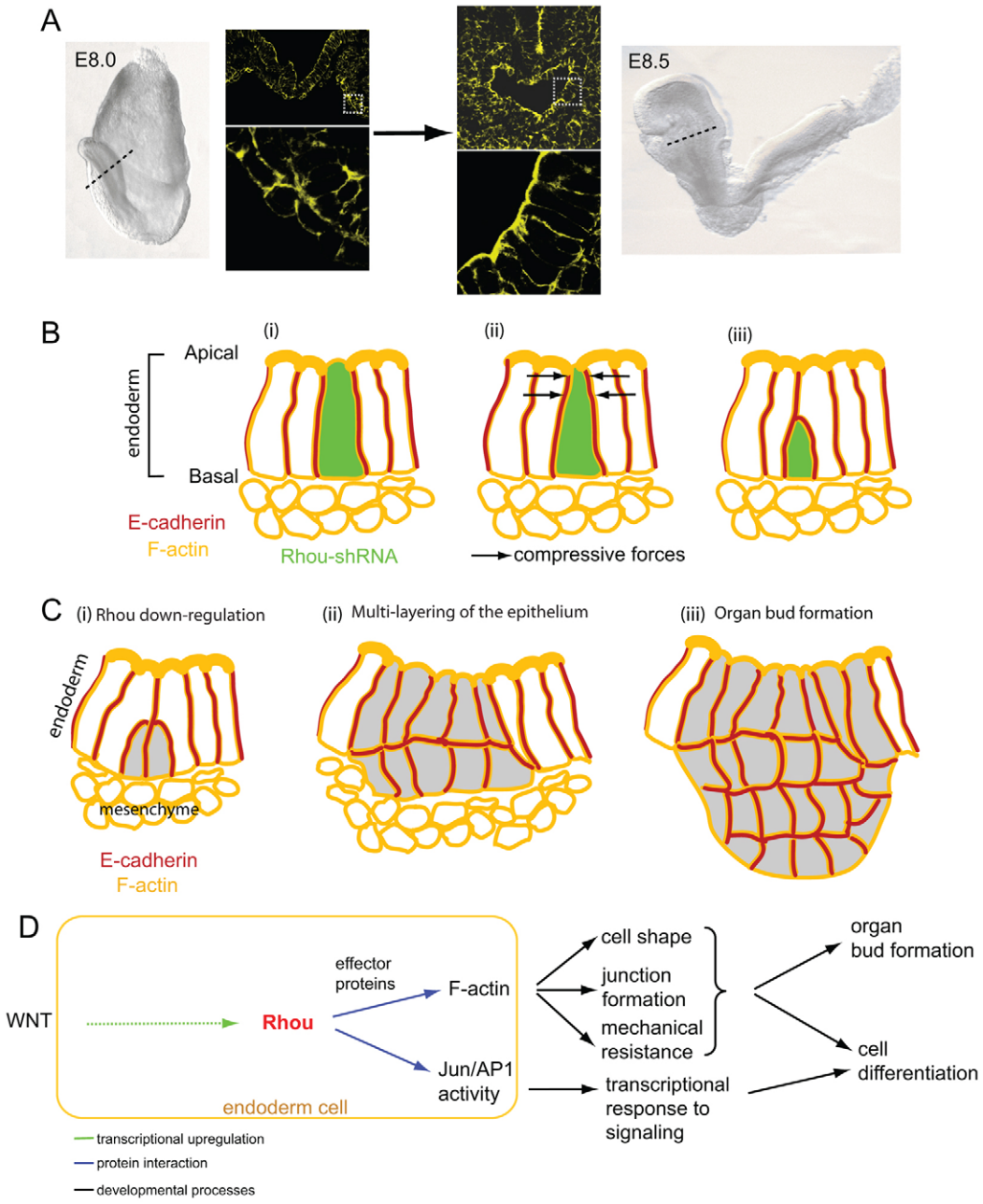

Fig. 7. F-actin localization and epithelial structure in the foregut endoderm, and the effects of Rhou depletion on cellular behaviour. (**A**) Phalloidin staining of the endoderm cells lining the foregut region of E8.0 and E8.5 embryos (plane of sectioning indicated by dashed lines). Higher magnification images of the boxed area show the transition of the definitive endoderm from a squamous epithelium with peripheral F-actin distribution to columnar epithelium with apically polarized F-actin distribution as the anterior intestinal portal forms. (**B**) Effects of depletion of *Rhou* on F-actin and the dislodgement of the cell from the apical surface of the epithelium: (i) Endoderm cell with reduced *Rhou* activity (green cell) does not maintain the apical regionalization of actin filaments. (ii) Reduction of apical actin filaments impacts on the ability of the cell to withstand the compressive forces from neighbouring epithelial cells. (iii) The *Rhou*-depleted cell succumbs to the physical forces and retracts to the basal region of the epithelium. (**C**) Organ bud formation by multilayering of the epithelium: (i) Cells that downregulate *Rhou* and have reduced apical of F-actin are forced out from the apical territory of the epithelium. (ii) Recruitment of additional cells to the basal layer and proliferation of cells generate the multi-layered foci that herald (iii) the formation of organ bud. (**D**) *Rhou* transcription is enhanced by Wnt signalling, probably indirectly. Rhou interacts with effector proteins in regulating the distribution of F-actin, influencing cell shape and mechanical properties, and activity of the AP-1 transcription factor complex, which, in turn, initiates the formation of organ primordia and cell differentiation.

for cellular stiffness and resistance to compressive forces (Jonas and Duschl, 2010; Oberleithner et al., 2009). Loss of apical F-actin in endoderm cells (Fig. 7B) might reduce the resistance of the cell to the compressive forces from surrounding cells and results in the cell being forced out of the apical/luminal domain. Overall, our findings suggest that Rhou affects the morphology of the endoderm cells via its action on the distribution of the actin and α-tubulin-enriched cytoskeleton.

The primordia of endoderm-derived organs are formed by budding of the epithelium. Budding of the thyroid, liver, lung and pancreas primordia begins by a thickening of the simple columnar epithelium, followed by pseudostratification and outgrowing from the foregut (Bort et al., 2006; Fagman et al., 2003). Bud formation from an epithelial tissue involves changes in cell shape including apical constriction, cytoskeletal rearrangement and epithelial sheet folding (Fagman and Nilsson, 2010; Pilot and Lecuit, 2005). These processes are associated with the formation of the thyroid diverticulum (Fagman and Nilsson, 2010; Hilfer et al., 1977). *Rhou* is downregulated in the ventral pharyngeal endoderm as the thyroid primordium forms, and knockdown of *Rhou* in embryos does not prevent the formation of organ buds. Rather, the thyroid primordium appeared enlarged in *Rhou* KD embryos, suggesting that the precocious loss of Rhou function expedites the morphogenesis of an organ bud.

The re-positioning of cells harbouring *Rhou* shRNAs towards the basal side of the epithelium (Fig. 7B) is reminiscent of the initiation of epithelial invagination. Our finding suggests a mechanism of the initiation of organ bud formation from the endoderm (Fig. 7C). As *Rhou* is downregulated in the presumptive organ bud, cells lose apical F-actin and are consequently sequestered into the basal part of the epithelium, resulting in the formation of a multilayered cell sheet. The cellular mass might expand, by recruitment of more Rhou-downregulated cells from the adjacent endoderm as well as the proliferation of cells in the multilayered sheet (Fagman and Nilsson, 2010), to form the organ bud (Fig. 7C). It is, therefore, possible that the timing and the domain of downregulation of *Rhou* in the ventral foregut endoderm might determine the schedule and site of organ bud formation during gut development.

Canonical Wnt signalling contributes to the regulation of *Rhou* in the embryo, but *Rhou* is not a direct transcriptional target of β-catenin, and is instead probably regulated via a JNK-mediated pathway (Schiavone et al., 2009; Tao et al., 2001). The results of this and other studies on the molecular mechanism of Rhou action highlight a likely connection between Wnt signalling, epithelial morphogenesis and the formation of organ primordia via Rhou-mediated changes to the cytoskeleton that affect cell shape and mechanical properties (Fig. 7D). Rhou activates JNK, as indicated by c-Jun phosphorylation (Chuang et al., 2007; Tao et al., 2001) and activity of the AP-1 transcription factor complex of which c-Jun forms a part (Zhang et al., 2011). Our ES cell differentiation data show that *Rhou* knockdown reduces the expression of targets of c-Jun/AP-1, including Wnt5a. JNK activity is required for normal expression of some endoderm lineage markers in differentiating EBs (see Fig. S4 in the supplementary material). JNK also acts via transcription-independent mechanisms to mediate the effects of Wnt on planar cell polarity/convergent extension during *Xenopus* development (Yamanaka et al., 2002) and regulation of epithelial morphogenesis, including the control of actin polymerization (Bogoyevitch and Kobe, 2006; Xia and Karin, 2004). This supports a connection between Wnt signalling and the regulation of the activity of components of the PCP/JNK pathway (Fig. 7D) and constitutes a novel mechanism whereby the transcriptional regulation of *Rhou* acts as the conduit for Wnt signalling activity to control cell and tissue morphogenesis and, subsequently, cell differentiation and organ bud formation.

Acknowledgements
We thank Andreas Kispert and Andy McMahon for the Wnt-expressing cell lines; Heiko Lickert for providing the RasGAP shRNA vector; Anne Blangy for the GFP-RHOU clone; Duncan Sparrow for the *Apom* cDNA and Rulang Jiang for the *Pax9* cDNA; Angelyn Hor for histology; Evelyn Trounson for assistance with cell culture; Ross Boadle and Laurence Cantrill for assistance with microscopy; Sanda Lum and Maggie Wang for cell sorting; and staff of the CMRI BioServices Unit for animal care. Animal experimentation was approved by the CMRI/CHW Animal Care and Ethics Committee.

Funding
This work was supported by the NHMRC of Australia (grant 323704), the Australian Research Council (grant DP0985052) and Mr James Fairfax. DAFL is a Kimberly Clark Research Fellow, N.F. is a University of Sydney Post-Doctoral Fellow and P.P.L.T. is a NHMRC Senior Principal Research Fellow (grant 372102).

Competing interests statement
The authors declare no competing financial interests.

Supplementary material
Supplementary material for this article is available at
http://dev.biologists.org/lookup/suppl/doi:10.1242/dev.063867/-/DC1

References

Aspenstrom, P., Fransson, A. and Saras, J. (2004). Rho GTPases have diverse effects on the organization of the actin filament system. *Biochem. J.* **377**, 327-337.
Bildsoe, H., Loebel, D. A., Jones, V. J., Chen, Y. T., Behringer, R. R. and Tam, P. P. (2009). Requirement for Twist1 in frontonasal and skull vault development in the mouse embryo. *Dev. Biol.* **331**, 176-188.
Bogani, D., Warr, N., Elms, P., Davies, J., Tymowska-Lalanne, Z., Goldsworthy, M., Cox, R. D., Keays, D. A., Flint, J., Wilson, V. et al. (2004). New semidominant mutations that affect mouse development. *Genesis* **40**, 109-117.
Bogoyevitch, M. A. and Kobe, B. (2006). Uses for JNK: the many and varied substrates of the c-Jun N-terminal kinases. *Microbiol. Mol. Biol. Rev.* **70**, 1061-1095.
Bort, R., Signore, M., Tremblay, K., Martinez Barbera, J. P. and Zaret, K. S. (2006). Hex homeobox gene controls the transition of the endoderm to a pseudostratified, cell emergent epithelium for liver bud development. *Dev. Biol.* **290**, 44-56.
Brady, D. C., Alan, J. K., Madigan, J. P., Fanning, A. S. and Cox, A. D. (2009). The transforming Rho family GTPase Wrch-1 disrupts epithelial cell tight junctions and epithelial morphogenesis. *Mol. Cell. Biol.* **29**, 1035-1049.
Chuang, Y. Y., Valster, A., Coniglio, S. J., Backer, J. M. and Symons, M. (2007). The atypical Rho family GTPase Wrch-1 regulates focal adhesion formation and cell migration. *J. Cell Sci.* **120**, 1927-1934.
D'Amour, K. A., Agulnick, A. D., Eliazer, S., Kelly, O. G., Kroon, E. and Baetge, E. E. (2005). Efficient differentiation of human embryonic stem cells to definitive endoderm. *Nat. Biotechnol.* **23**, 1534-1541.
Fagman, H. and Nilsson, M. (2010). Morphogenesis of the thyroid gland. *Mol. Cell. Endocrinol.* **323**, 35-54.
Fagman, H., Grande, M., Edsbagge, J., Semb, H. and Nilsson, M. (2003). Expression of classical cadherins in thyroid development: maintenance of an epithelial phenotype throughout organogenesis. *Endocrinology* **144**, 3618-3624.
Fort, P., Guemar, L., Vignal, E., Morin, N., Notarnicola, C., de Santa, B. P. and Faure, S. (2011). Activity of the RhoU/Wrch1 GTPase is critical for cranial neural crest cell migration. *Dev. Biol.* **350**, 451-463.
Fossat, N., Jones, V., Khoo, P. L., Bogani, D., Hardy, A., Steiner, K., Mukhopadhyay, M., Westphal, H., Nolan, P. M., Arkell, R. et al. (2011). Stringent requirement of a proper level of canonical WNT signalling activity for head formation in mouse embryo. *Development* **138**, 667-676.
Franklin, V., Khoo, P. L., Bildsoe, H., Wong, N., Lewis, S. and Tam, P. P. (2008). Regionalisation of the endoderm progenitors and morphogenesis of the gut portals of the mouse embryo. *Mech. Dev.* **125**, 587-600.
Hansson, M., Olesen, D. R., Peterslund, J. M., Engberg, N., Kahn, M., Winzi, M., Klein, T., Maddox-Hyttel, P. and Serup, P. (2009). A late requirement for Wnt and FGF signaling during activin-induced formation of foregut endoderm from mouse embryonic stem cells. *Dev. Biol.* **330**, 286-304.
Harris, T. J., Sawyer, J. K. and Peifer, M. (2009). How the cytoskeleton helps build the embryonic body plan: models of morphogenesis from *Drosophila*. *Curr. Top. Dev. Biol.* **89**, 55-85.
Hilfer, S. R., Palmatier, B. Y. and Fithian, E. M. (1977). Precocious evagination of the embryonic chick thyroid in ATP-containing medium. *J. Embryol. Exp. Morphol.* **42**, 163-175.
Hou, J., Charters, A. M., Lee, S. C., Zhao, Y., Wu, M. K., Jones, S. J., Marra, M. A. and Hoodless, P. A. (2007). A systematic screen for genes expressed in definitive endoderm by Serial Analysis of Gene Expression (SAGE). *BMC Dev. Biol.* **7**, 92.
Jia, Y., Yang, Y., Liu, S., Herman, J. G., Lu, F. and Guo, M. (2010). SOX17 antagonizes WNT/beta-catenin signaling pathway in hepatocellular carcinoma. *Epigenetics* **5**, 743-749.

Johnson, M., Sharma, M., Jamieson, C., Henderson, J. M., Mok, M. T. S., Bendall, L. and Henderson, B. R. (2009). Regulation of [beta]-catenin trafficking to the membrane in living cells. *Cell. Signal.* **21**, 339-348.
Jonas, O. and Duschl, C. (2010). Force propagation and force generation in cells. *Cytoskeleton* **67**, 555-563.
Kanai-Azuma, M., Kanai, Y., Gad, J. M., Tajima, Y., Taya, C., Kurohmaru, M., Sanai, Y., Yonekawa, H., Yazaki, K., Tam, P. P. et al. (2002). Depletion of definitive gut endoderm in Sox17-null mutant mice. *Development* **129**, 2367-2379.
Khoo, P. L., Franklin, V. J. and Tam, P. P. L. (2007). Fate-mapping technique: targeted whole-embryo electroporation of DNA constructs into the germ layers of mouse embryos 7-7.5 days post-coitum. *Cold Spring Harb. Protoc.* **2007**, pdb.prot4893.
Kinder, S. J., Tan, S. S. and Tam, P. P. L. (2000). Cell grafting and fate mapping of the early-somite-stage mouse embryo. *Methods Mol. Biol.* **135**, 425-437.
Kispert, A., Vainio, S. and McMahon, A. P. (1998). Wnt-4 is a mesenchymal signal for epithelial transformation of metanephric mesenchyme in the developing kidney. *Development* **125**, 4225-4234.
Kubo, A., Shinozaki, K., Shannon, J. M., Kouskoff, V., Kennedy, M., Woo, S., Fehling, H. J. and Keller, G. (2004). Development of definitive endoderm from embryonic stem cells in culture. *Development* **131**, 1651-1662.
Kunath, T., Gish, G., Lickert, H., Jones, N., Pawson, T. and Rossant, J. (2003). Transgenic RNA interference in ES cell-derived embryos recapitulates a genetic null phenotype. *Nat. Biotechnol.* **21**, 559-561.
Lawson, K. A., Meneses, J. J. and Pedersen, R. A. (1986). Cell fate and cell lineage in the endoderm of the presomite mouse embryo, studied with an intracellular tracer. *Dev. Biol.* **115**, 325-339.
Lickert, H., Cox, B., Wehrle, C., Taketo, M. M., Kemler, R. and Rossant, J. (2005). Dissecting Wnt/beta-catenin signaling during gastrulation using RNA interference in mouse embryos. *Development* **132**, 2599-2609.
Loebel, D. A., Tsoi, B., Wong, N., O'Rourke, M. P. and Tam, P. P. (2004). Restricted expression of ETn-related sequences during post-implantation mouse development. *Gene Expr. Patterns* **4**, 467-471.
Miranda-Saksena, M., Armati, P., Boadle, R. A., Holland, D. J. and Cunningham, A. L. (2000). Anterograde transport of herpes simplex virus type 1 in cultured, dissociated human and rat dorsal root ganglion neurons. *J. Virol.* **74**, 1827-1839.
Mukhopadhyay, M., Shtrom, S., Rodriguez-Esteban, C., Chen, L., Tsukui, T., Gomer, L., Dorward, D. W., Glinka, A., Grinberg, A., Huang, S. P. et al. (2001). Dickkopf1 is required for embryonic head induction and limb morphogenesis in the mouse. *Dev. Cell* **1**, 423-434.
Nagy, A., Gocza, E., Diaz, E. M., Prideaux, V. R., Ivanyi, E., Markkula, M. and Rossant, J. (1990). Embryonic stem cells alone are able to support fetal development in the mouse. *Development* **110**, 815-821.
Nolan, P. M., Peters, J., Strivens, M., Rogers, D., Hagan, J., Spurr, N., Gray, I. C., Vizor, L., Brooker, D., Whitehill, E. et al. (2000). A systematic, genome-wide, phenotype-driven mutagenesis programme for gene function studies in the mouse. *Nat. Genet.* **25**, 440-443.
Oberleithner, H., Callies, C., Kusche-Vihrog, K., Schillers, H., Shahin, V., Riethmuller, C., Macgregor, G. A. and de Wardener, H. E. (2009). Potassium softens vascular endothelium and increases nitric oxide release. *Proc. Natl. Acad. Sci. USA* **106**, 2829-2834.
Ofek, G., Wiltz, D. C. and Athanasiou, K. A. (2009). Contribution of the cytoskeleton to the compressive properties and recovery behavior of single cells. *Biophys. J.* **97**, 1873-1882.
Ory, S., Brazier, H. and Blangy, A. (2007). Identification of a bipartite focal adhesion localization signal in RhoU/Wrch-1, a Rho family GTPase that regulates cell adhesion and migration. *Biol. Cell* **99**, 701-716.
Pfister, S., Jones, V. J., Power, M., Truisi, G. L., Khoo, P. L., Steiner, K. A., Kanai-Azuma, M., Kanai, Y., Tam, P. P. and Loebel, D. A. (2011). Sox17-dependent gene expression and early heart and gut development in Sox17-deficient mouse embryos. *Int. J. Dev. Biol.* **55**, 45-58.
Pilot, F. and Lecuit, T. (2005). Compartmentalized morphogenesis in epithelia: from cell to tissue shape. *Dev. Dyn.* **232**, 685-694.
Qian, X., Samadani, U., Porcella, A. and Costa, R. H. (1995). Decreased expression of hepatocyte nuclear factor 3 alpha during the acute-phase response influences transthyretin gene transcription. *Mol. Cell. Biol.* **15**, 1364-1376.
Radonic, A., Thulke, S., Mackay, I. M., Landt, O., Siegert, W. and Nitsche, A. (2004). Guideline to reference gene selection for quantitative real-time PCR. *Biochem. Biophys. Res. Commun.* **313**, 856-862.
Saras, J., Wollberg, P. and Aspenstrom, P. (2004). Wrch1 is a GTPase-deficient Cdc42-like protein with unusual binding characteristics and cellular effects. *Exp. Cell Res.* **299**, 356-369.
Schiavone, D., Dewilde, S., Vallania, F., Turkson, J., Di, C. F. and Poli, V. (2009). The RhoU/Wrch1 Rho GTPase gene is a common transcriptional target of both the gp130/STAT3 and Wnt-1 pathways. *Biochem. J.* **421**, 283-292.
Tada, S., Era, T., Furusawa, C., Sakurai, H., Nishikawa, S., Kinoshita, M., Nakao, K., Chiba, T. and Nishikawa, S. (2005). Characterization of mesendoderm: a diverging point of the definitive endoderm and mesoderm in embryonic stem cell differentiation culture. *Development* **132**, 4363-4374.
Tam, P. P., Khoo, P. L., Lewis, S. L., Bildsoe, H., Wong, N., Tsang, T. E., Gad, J. M. and Robb, L. (2007). Sequential allocation and global pattern of movement of the definitive endoderm in the mouse embryo during gastrulation. *Development* **134**, 251-260.
Tao, W., Pennica, D., Xu, L., Kalejta, R. F. and Levine, A. J. (2001). Wrch-1, a novel member of the Rho gene family that is regulated by Wnt-1. *Genes Dev.* **15**, 1796-1807.
Tremblay, K. D. and Zaret, K. S. (2005). Distinct populations of endoderm cells converge to generate the embryonic liver bud and ventral foregut tissues. *Dev. Biol.* **280**, 87-99.
Vicente-Manzanares, M. and Sanchez-Madrid, F. (2000). Cell polarization: a comparative cell biology and immunological view. *Dev. Immunol.* **7**, 51-65.
Watson, C. M., Trainor, P. A., Radziewic, T., Pelka, G. J., Zhou, S. X., Parameswaran, M., Quinlan, G. A., Gordon, M., Sturm, K. and Tam, P. P. L. (2008). Application of lacZ transgenic mice to cell lineage studies. *Methods Mol. Biol.* **461**, 149-164.
Wilkinson, D. G. and Nieto, M. A. (1993). Detection of messenger RNA by in situ hybridization to tissue sections and whole mounts. *Methods Enzymol.* **225**, 361-373.
Xia, Y. and Karin, M. (2004). The control of cell motility and epithelial morphogenesis by Jun kinases. *Trends Cell Biol.* **14**, 94-101.
Xu, P. and Davis, R. J. (2010). c-Jun NH2-terminal kinase is required for lineage-specific differentiation but not stem cell self-renewal. *Mol. Cell. Biol.* **30**, 1329-1340.
Yamanaka, H., Moriguchi, T., Masuyama, N., Kusakabe, M., Hanafusa, H., Takada, R., Takada, S. and Nishida, E. (2002). JNK functions in the non-canonical Wnt pathway to regulate convergent extension movements in vertebrates. *EMBO Rep.* **3**, 69-75.
Zhang, J. S., Koenig, A., Young, C. and Billadeau, D. D. (2011). GRB2 couples RhoU to epidermal growth factor receptor signaling and cell migration. *Mol. Biol. Cell* **22**, 2119-2130.
Zorn, A. M. and Wells, J. M. (2009). Vertebrate endoderm development and organ formation. *Annu. Rev. Cell Dev. Biol.* **25**, 221-251.
Zorn, A. M., Barish, G. D., Williams, B. O., Lavender, P., Klymkowsky, M. W. and Varmus, H. E. (1999). Regulation of Wnt signaling by Sox proteins: XSox17 alpha/beta and XSox3 physically interact with beta-catenin. *Mol. Cell* **4**, 487-498.

Table S1. Comparison of the outcome of generation of ES-chimeara from the *Rhou*-knockdown embryonic stem (ES) cell lines

ES cell line	Blastocysts transferred (number of recipients)	Mean embryos per blastocyst transferred (± s.e.m.)	*P*-value (*t*-test)
control	203 (18)	0.144±0.040	
Rhou-809	106 (9)	0.153±0.033	0.89
Rhou-3130	148 (13)	0.137±0.043	0.89